ADVANCED MATERIALS
www.advmat.de

Acoustodynamic Covalent Materials Engineering for the Remote Control of Physical Properties Inside Materials

Satoshi Honda, Minami Oka, Kazuki Fuke, Pierre T. Khuri-Yakub, and Chi Nan Pai*

Advances in vat photopolymerization (VP) 3D printing (3DP) technology enable the production of highly precise 3D objects. However, it is a major challenge to create dynamic functionalities and to manipulate the physical properties of the inherently insoluble and infusible cross-linked material generated from VP-3DP without reproduction. The fabrication of light- and high-intensity focused ultrasound (HIFU)-responsive cross-linked polymeric materials linked with hexaarylbiimidazole (HABI) in polymer chains based on VP-3DP is reported here. Although the photochemistry of HABI produces triphenylimidazolyl radicals (TPIRs) during the process of VP-3DP, the orthogonality of the photochemistry of HABI and photopolymerization enables the introduction of reversible cross-links derived from HABIs in the resulting 3D-printed objects. While photostimulation cleaves a covalent bond between two imidazoles in HABI to generate TPIRs only near the surface of the 3D-printed objects, HIFU triggers cleavage in the interior of materials. In addition, HIFU travels beyond an obstacle to induce a response of HABI-embedded cross-linked polymers, which cannot be attainable with photostimulation. The present system would be beneficial for tuning the physical properties and recycling of various polymeric materials, but it will also open the door for pinpoint modification, healing, and reshaping of materials when coupled to various dynamic covalent materials.

1. Introduction

3D printing (3DP) technologies continue to grow scientifically and industrially and lead to new implementations in various areas.[1] Among a wide variety of 3DP technologies, vat photopolymerization (VP)-based processes applied to stereolithography (SLA), digital light processing (DLP), and liquid crystalline display (LCD) 3D printers enable the fabrication of a more complex 3D object with a higher resolution and a lower feature size compared to the fused deposition modeling (FDM) process.[2] The process of VP-3DP uses monomers, oligomers, and cross-linkers with polymerization sites in the liquid state that undergo polymerization in the presence of either photoradical or photocation generators upon exposure to light.[1b] This leads to a great opportunity for synthetic organic chemists, as the development of new functional molecules is directly linked to the fabrication of unprecedented functional 3D objects, which could also be the final products with expected applications.[2a,3] However, two major challenges remain in this area.

One is to fabricate stimuli-responsive 3D objects by dynamic covalent materials (DCMs).[4] Emerging reports have mainly focused on thermoresponsive motifs to manipulate the physical properties of whole 3D-printed objects, as represented by the Diels–Alder reaction.[5] While photostimulation is attractive in that it can achieve spatially and temporally local responses, the use of photoresponsive DCMs has been limited due to their inherent photoreactivity that generally interferes with VP processes. The key for fabricating photoresponsive 3D-printed objects is the effective use of photoreactions orthogonal to photopolymerization reactions, as represented by the reversible photocycloaddition of anthracene,[6] which does not generate radical species. On the other hand, dimer formation and dissociations based on reversible radical coupling reactions are also known, allowing for a distinct photoresponsive system from photocycloaddition reactions.[7] How, then, are we able to realize VP-3DP of photoresponsive objects that can manipulate properties based on photoreversible radical coupling reactions? In this context, we focused on the photoreaction of hexaarylbiimidazole (HABI). One of the beginnings of research regarding the photochemistry of HABI dates back to 1960 at DuPont, where the chemistry has now been industrialized as a practical photopolymerization system.[8] Upon photoirradiation, HABI reversibly produces

S. Honda, M. Oka, K. Fuke
Department of Basic Science
Graduate School of Arts and Sciences
The University of Tokyo
3-8-1 Komaba, Meguro, Tokyo 153-8902, Japan
E-mail: c-honda@mail.ecc.u-tokyo.ac.jp
P. T. Khuri-Yakub
E. L. Ginzton Laboratory
Stanford University
348 Via Pueblo Mall, Stanford, CA 94305, USA
C. N. Pai
Department of Mechatronics and Mechanical Systems Engineering
Polytechnic School of the University of Sao Paulo
Avenida Professor Mello Moraes 2231, Sao Paulo 05508-030, Brazil

The ORCID identification number(s) for the author(s) of this article can be found under https://doi.org/10.1002/adma.202304104

DOI: 10.1002/adma.202304104

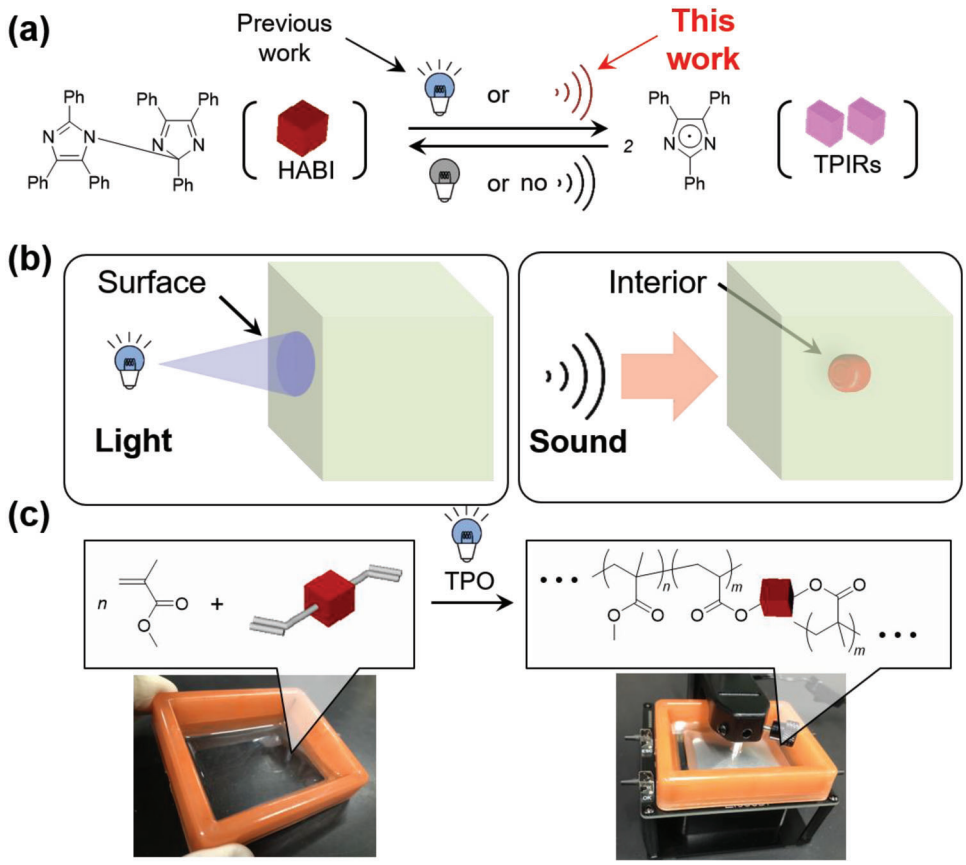

Figure 1. a) Photochemistry of HABI. b) Conceptual illustrations of material responses triggerable by light (left) and ultrasound (right) stimulations. c) Fabrication of 3D opjects by VP-3DP based on orthogonality of the photopolymerization and photoreaction of HABI.

a pair of 2,4,5-triphenylimidazoryl radicals (TPIRs)[9] (**Figure 1**a). It is well known that while the produced TPIR does not undergo electrophilic radical addition to double bonds, it can abstract hydrogen from a hydrogen donor.[10] In the presence of a chain transfer agent (CTA) such as thiol, TPIR reacts with the CTA, and then a produced secondary radical species derived from the CTA initiates radical polymerization of various vinyl monomers.[8] The concept of using HABI as a photoradical generator continuously encourages the development of photoreaction systems such as a thiol–ene reaction for dental restorative materials[11] and radical reactions with silica-supported HABI-containing cross-linked copolymers as heterogeneous radical generators,[12] to mention a few. In contrast, in the absence of CTAs, TPIR generated upon photoirradiation reacts with other TPIRs to revert back to HABI again. This reversible photochemistry also finds applications for photochromic materials with fast responses[13] and polymer fluids[7b] and elastomers with phototunable viscoelasticity.[14] Considering that HABI has been used for photopolymerization, it is seemingly difficult to fabricate a 3D object without reacting HABI in VP-3DP processes. However, we hypothesized that if the photopolymerization reaction is orthogonal to the photoreaction of HABI in the absence of CTA, it would be possible to fabricate a 3D object containing photoresponsive HABI with VP-3DP processes.

The second major challenge is to develop a facile methodology to dismantle or degrade cross-linked materials produced upon VP-3DP processes after end-of-use. To this end, stimuli-responsive polymers are receiving increased attention for achieving a circular economy.[5a] Similar to the aforementioned challenge, photoreversible bonding is effective when only the photoirradiated area is to be responded to. However, since light can only act on the surface of a material, it cannot respond to a target deep within the material or across an obstacle (Figure 1b, left). To overcome this, we focused on the effective utilization of high-intensity focused ultrasound (HIFU).[15] Ultrasound is a type of mechanical wave that can be generated by a vibrating source. Multiple waves with crossing paths may present constructive or destructive interferences, resulting in stronger or weaker waves. When an ultrasound transducer is designed so that all the created waves propagate to converge at a single point, which is called the focal point, higher energy can be achieved at this point.[15] In contrast to other types of high intensity ultrasounds, HIFU only presents higher energy at the focal point. Because of this particularity, HIFU has been clinically researched and used, for example, as a noninvasive advanced medical treatment for cancer.[16] In related studies, HIFU-triggered disassembly of carriers composed of block copolymers for drug delivery and to induce the release of drugs incorporated in such carriers has been studied over a decade.[17] However, unlike usual ultrasound, which has been historically applied to polymers and has established the field of mechanochemistry,[18] the utilization of HIFU for bulk materials in the solid-state is still considered nascent.[19]

Encouraging reports to this end applied flexible mechanoluminescent poly(dimethylsiloxane) (PDMS) with 1, 2-dioxetane in the chains,[20] and poly(ethylene glycol) gels embedded with azo mechanophores.[21] Although these reactions are not reversible, it is noteworthy that HIFU can cleave flexible polymer chains to generate a fluorescent motif in rubbery materials or gels. From these attractive features of HIFU and growing interests in the related field, we envisioned that the energy produced with HIFU can cleave the covalent bond between the two imidazoles in HABI in grassy solid-state cross-linked materials (Figure 1a) and that HIFU has the potential to remotely manipulate the physical properties of targets inside materials or beyond obstacles (Figure 1b, right).

Herein, we demonstrate these hypotheses. We synthesized HABI-appended cross-linkers and used them for photopolymerization. Owing to the orthogonality of the photopolymerization and photoreaction of HABI, efficient fabrication of photoresponsive 3D-printed objects with reversibly photocleavable cross-links derived from HABIs has been successfully achieved using an inexpensive 3D printer (Figure 1c). When the 3D-printed object was exposed to light, the surface color changed immediately owing to the production of TPIRs from HABI, and the storage modulus (G') of the object reversibly decreased upon ON-OFF cycles of photoirradiation. In contrast, when a 3D-printed object was sonicated with a HIFU transducer, the material at the focal point, located at the interior of the object, responded, and the 3D-printed object was easily broken down with a higher input voltage to the HIFU transducer. With a lower input voltage, the G' of the object reasonably decreased immediately after HIFU sonication. Furthermore, HIFU traveled through a silicone opaque obstacle and induced a response in the HABI-embedded 3D-printed object. Such manipulation of properties inside materials is usually unattainable with photostimulation, but we were able to prove that HIFU is an effective means for dismantling cross-linked polymeric materials and inducing reversible radical coupling reactions.

2. Results and Discussion

2.1. Synthesis of Cross-linkers and their Use in Thermal Free Radical Polymerization

We first synthesized HABI-containing diacrylates and dimethacrylates (**4**, **5**, **10**, **11**, and **16**) to test the generality in designing cross-linkers (**Figure 2**a), where the cross-linkers and their precursors have thoroughly been characterized (Figures S1–S8, Supporting Information). Among them, the synthesis of **4** and **5** was easiest, but these phenyl ester-type cross-linkers were labile in air at room temperature. While the synthesis of **10** and **11** requires an additional etherification step compared to those of **4** and **5**, they were sufficiently stable in air and had good storage stability at room temperature. Although more steps are required to obtain **16**, which was synthesized for the purpose of showing that the position of substituents can be arbitrarily determined, it is obvious from these synthetic examples that there is a high degree of design flexibility in the synthesis of HABI-containing cross-linkers. These compounds were then used as cross-linkers for typical thermal free-radical polymerization (FRP) of methyl methacrylate (MMA) with a low-temperature initiation system using benzoyl peroxide (BPO) and *N,N*-dimethyl-*p*-toluidine (DMT) at 40 °C (Figure 2b). Effective incorporation of these cross-linkers was readily confirmed by the production of polymerized materials insoluble in organic solvents. Our interest is whether the incorporated HABIs maintain photoreactivity in the cross-linked PMMA. In this context, the apparent change in the color of materials upon the production and consumption of TPIRs triggered by the photoreaction of HABI would enable visual evaluation of its incorporation. Upon photoirradiation, the light-yellow cross-linked PMMA in the glassy state only in the irradiated region turned dark blue at room temperature (Figure 2c), again indicating the insertion of the cross-linker into the polymer chains.

2.2. Photoinitiated Free Radical Polymerization and Vat Photopolymerization 3D Printing

Encouraged by these findings, we proceeded with a photoinitiated FRP system. We selected the photopolymerization of MMA in the presence of diphenyl(2,4,6-trimethylbenzoyl)phosphine oxide (TPO) and *o*-Cl-HABI as a model reaction (**Figure 3**a). TPO has been selected as a photoinitiator because of its effective absorption of light around the emission wavelength of LEDs (λ = 405 nm) equipped with 3D printers.[1a] The photopolymerization product was thoroughly analyzed based on atmospheric pressure chemical ionization (APCI)-MS spectrometry. The APCI-MS spectrum of the photopolymerization product showed peaks derived from *o*-Cl-HABI (m/z = 659.1) and oligo(MMA)s (m/z = 301.0, 401.0, 501.0, and 601.0) with a peak interval of 100, which exactly corresponds to the molar mass of MMA (Figure 3b). In addition, the appearance of the lophine-derived high-intensity peak (m/z = 331.1) suggests the cleavage of *o*-Cl-HABI into *o*-Cl-TPIRs and subsequent protonation in the ionization process of APCI-MS. This also suggests that the generated TPIR did not cause the initiation of photopolymerization; the absence of oligomer-derived peaks initiated from *o*-Cl-TPIR on the spectrum also supports that *o*-Cl-TPIR was not involved in photopolymerization. Considering that the production of TPIR causes strong visible light absorption, as evidenced by the comparison of UV–vis spectra between *o*-Cl-HABI and *o*-Cl-TPIR (Figure 3c) and the significant change in the color of their solutions (Movie S1 and Figure S9, Supporting Information), the orthogonality of these two photoreactions can, in principle, be monitored by the visible color change. We therefore monitored changes in color throughout photopolymerization (Movie S2, Supporting Information). During photopolymerization, the yellow color of the solution before the reaction (Figure 3d) first turned into TPIR-derived pink color during photoirradiation, and there was a pink color immediately after terminating photoirradiation (t = 0) (Figure 3e). At 90 s after terminating photoirradiation, a slight pink color remained (Figure 3f), but after 180 s, the coloration had almost disappeared (Figure 3g). If TPIR works as an initiator, this pink coloration should immediately disappear after the initiation reaction. Therefore, this observation again supports the orthogonality of the present photopolymerization reaction and the photochemistry of HABI.

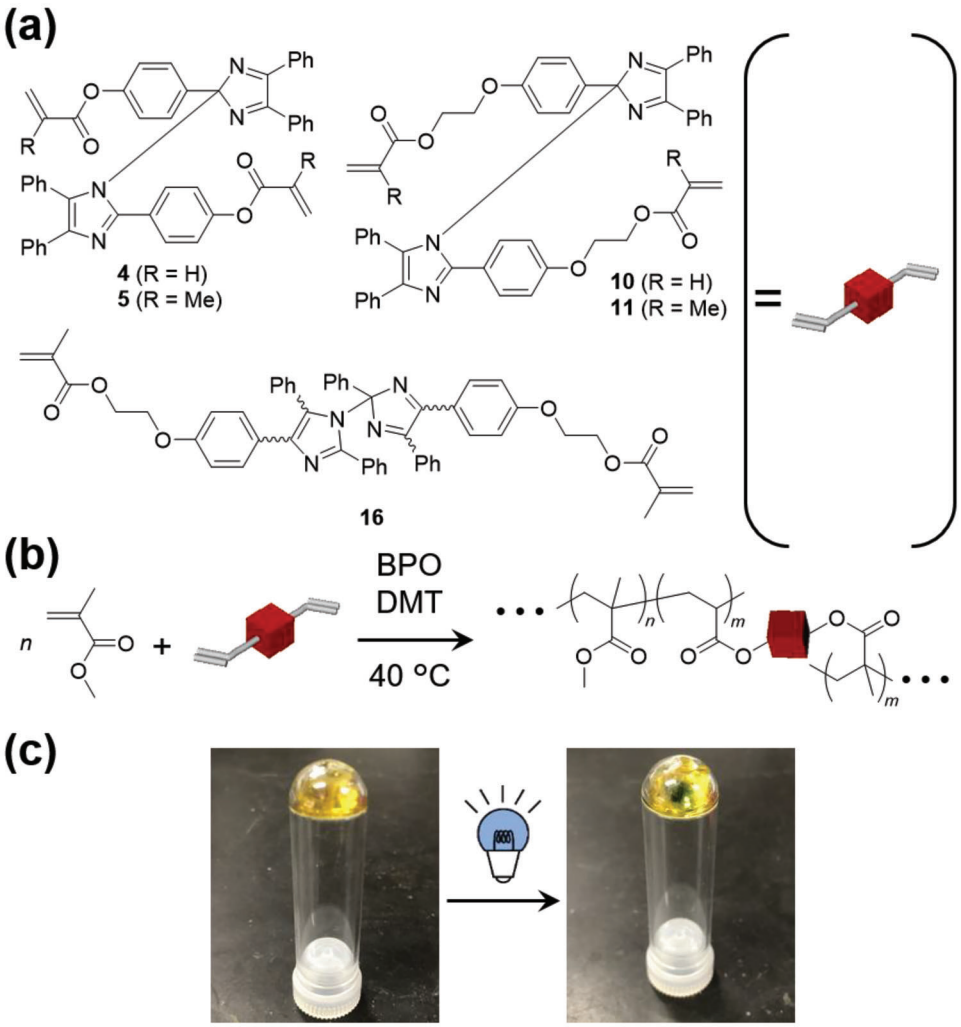

Figure 2. a) Chemical structures of cross-linkers containing photoresponsive HABIs. b) Thermal FRP of MMA and cross-linkers containing photoresponsive HABIs initiated by benzoyl peroxide in the presence of *N*,*N*-dimethyl-*p*-toluidine as a low-temperature polymerization accelerator. c) Photographs of the cross-linked material produced upon thermal FRP of MMA and **11** before (left) and after (right) photoirradiation.

We selected methacrylate-based **11** for further study, and VP-3DP based on the photopolymerization of a mixture of MMA, bis-GMA, and **11** initiated with TPO was conducted (**Figure 4**a). Our preliminary studies indicated that mixing with monomers capable of dissolving powder-state **11** is a prerequisite, and **11** dissolved in MMA up to 50 wt.%. However, the photocuring reaction of a mixture of **11** and MMA (**11**/MMA = 50/50, w/w) with TPO as the initiator did not proceed upon photoirradiation (λ = 405 nm). This is likely due to the simultaneous cleavage of HABI to produce radical species (**11***), disturbing the formation of cross-links during photopolymerization. In fact, comparison of UV–vis absorption spectra between **11** and TPO shows that these have comparable absorptions at ≈400 nm, and the absorption of **11** ranges to ≈490 nm even with the same concentration as TPO (Figure S10, Supporting Information). It would no longer be a typical LED wavelength or photoinitiator for 3D printing, but it would be possible to 3D print such a mixture upon photoirradiation (λ = 490 nm) using initiators that can absorb 490 nm. After screening various initiators, we found that a recently developed photoinitiation system using a mixture of (±)-camphorquinone (CQ) and 2-(dimethylamino)ethyl methacrylate (DAEMA) in combination with diphenyliodonium hexafluorophosphate (DPIH)[22] has strong absorption at ≈490 nm (Figure S10, Supporting Information). From time-dependent rheological analysis upon photoirradiation, the photopolymerization mixture using TPO as the initiator upon photoirradiation (λ = 405 and 495 nm) showed a slight increase in storage modulus (G') while maintaining its liquid state (Figure S11, Supporting Information, blue square and black circle). In contrast, photopolymerization using a mixture of CQ, DAEMA, and DPIH as the initiation system, showed a two-order increase in G' upon photoirradiation (λ = 495 nm) (Figure S11, Supporting Information, red rectangle). Therefore, while not printable by readily available 3D printers, the mixture of **11** and MMA has potential as a fully recyclable and reversible material for 3DP.

Meanwhile, we mixed bis-GMA as a permanent cross-linker with a chemical structure relatively similar to **11**. While bis-GMA

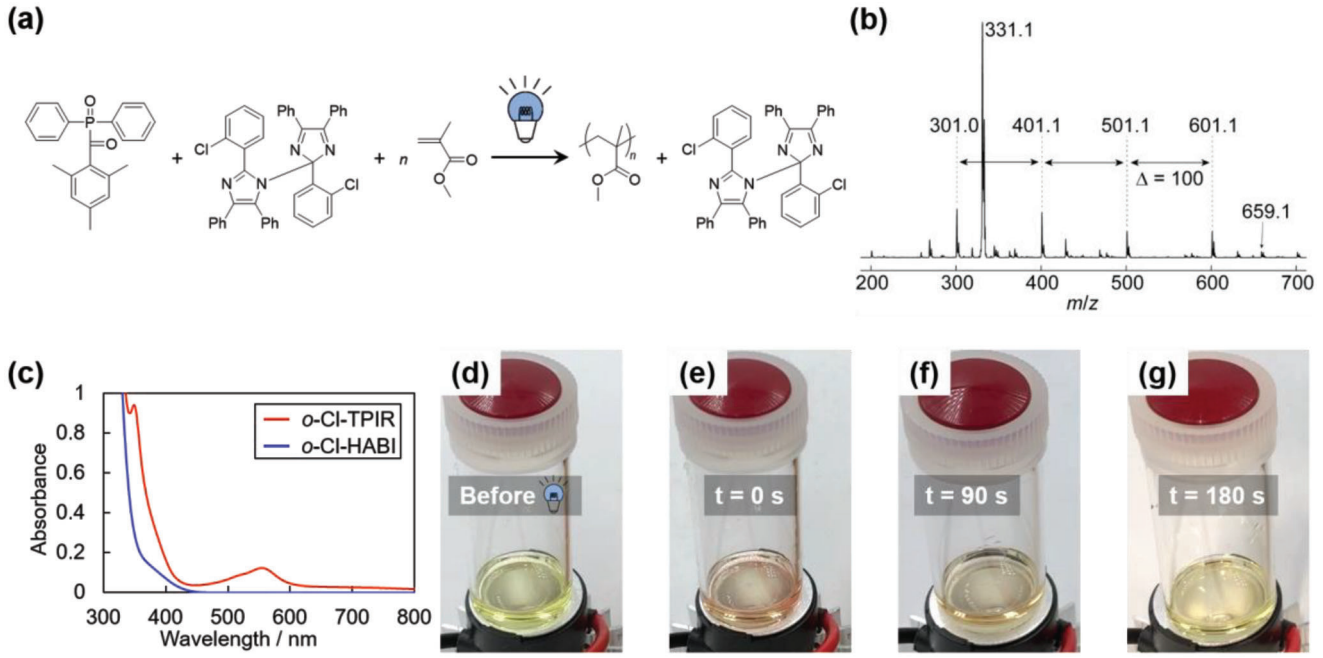

Figure 3. a) Photopolymerization of MMA in the presence of TPO and *o*-Cl-HABI. b) APCI-MS spectrum of the product after photopolymerization of MMA in the presence of TPO and *o*-Cl-HABI. c) UV–vis absorption spectra of *o*-Cl-HABI (blue) and *o*-Cl-TPIR (red) The concentration was 0.1 mg mL^{-1}. d–g) Photographs of the color of the reaction mixture during photopolymerization. The photographs were taken from Movie S2 (Supporting Information) at given times.

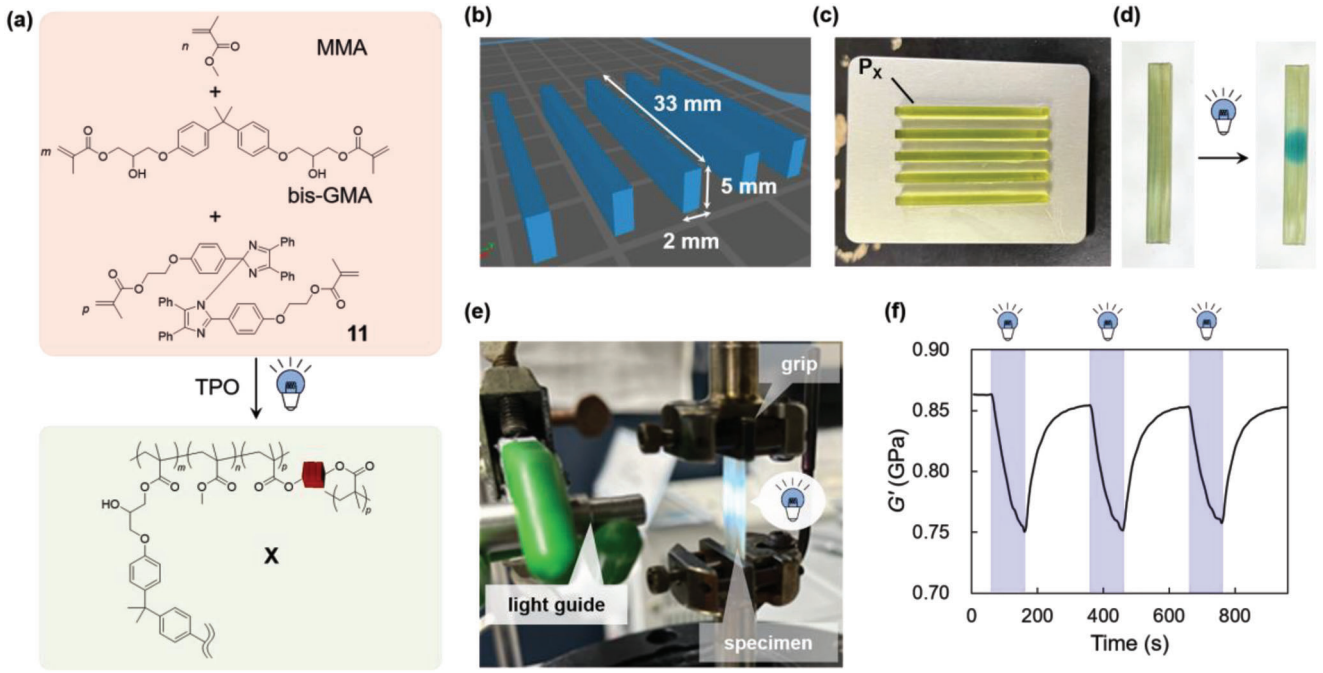

Figure 4. a) Photopolymerization reaction applied for VP-3DP. b) 3D data of the flexural test specimen and its dimensions. c–e) Photographs of the platform after VP-3DP (c), the 3D-printed object before (left) and after (right) photoirradiation (d), and the experimental setup for DMA upon photoirradiation (e). f) Time-course plots of *G'* upon photoirradiation. The photoirradiated time ranges were indicated with blue shades.

did not dissolve **11**, a three-component mixture of bis-GMA, MMA, and **11** was homogeneous, suggesting its applicability for VP-3DP. As preliminary photoirradiation experiments using an LED lamp ($\lambda = 405$ nm) indicated that photocuring of a mixture containing over 10 wt% of **11** took more than 3 min for each layer, we selected the mixture containing 2.5 wt% of **11** for further study, which required 45 s for photocuring each layer with an affordable 3D printer. We created CAD data of cuboids with dimensions of 33 mm × 5 mm × 2 mm (Figure 4b) and subjected them to VP-3DP. Highly precise 3D-printed objects (**X**) were readily obtained, as evident from the photograph of the platform after finishing the printing and subsequent washing processes (Figure 4c). The averaged flexural modulus (E_f) determined based on three-point bending flexural tests was 2.72 ± 0.22 GPa, which is in the range of those of photoresins used for mechanical applications.[2a] Importantly, **X** showed a prominent response to light ($\lambda = 405$ nm) with a color change from light yellow to blue only in the irradiated area, demonstrating explicit 3D printability of stiff objects while maintaining the photoresponsivity of HABIs (Figure 4d). To elucidate the effect of photoirradiation on mechanical properties, a setup for dynamic mechanical analysis (DMA) in torsion mode that enables photoirradiation during the measurements was constructed (Figure 4e). Time-course plots of G' upon ON–OFF cycles of photoirradiation showed repetitive decreases and increases in G' (Figure 4f). These changes reveal not only photoreversibility in dynamic mechanical properties but also that G' decreases by 0.11 GPa upon photostimulation, even though **X** has a G' of 0.87 GPa. Notably, the difference in G' between the photoirradiated (0.87 GPa) and nonirradiated states (0.76 GPa) reaches 10% despite containing only 2.5% of photoresponsive **11**. Therefore, by taking advantage of the orthogonality of photopolymerization and the photochemistry of HABI, we succeeded in fabricating cross-linked polymers containing **11** based on VP-3DP while maintaining the photoresponsivity of HABI in the printed objects.

2.3. HIFU Sonication for the Dismantling and Tuning of Mechanical Properties with HABI-Containing 3D-Printed Objects

Considering that conventional VP-3DP processes produce cross-linked polymers that are insoluble and infusible and whose properties, in principle, cannot be controlled once formed, the development of a methodology that enables the tuning of their properties only at a desired part after VP-3DP would be attractive. In our previous study, pinpoint control of material properties was achieved mainly by using photostimulation,[7a,14a] which can only control properties on the surface of materials, yet control of properties inside the material at a desired position has been a longstanding challenge. Inspired by the fact that the molecular weight of PDMS with HABIs in the polymer chains shifts in response to ultrasound,[7b] we envisioned the possibility of controlling local physical properties inside 3D-printed materials if we could focus ultrasound waves traveling over obstacles that light cannot transmit.

We thus fabricated a HIFU transducer consisting of an aluminum body, focal lens, and piezoelectric ceramic (PZT) disk (ϕ25.0 mm) with a resonance frequency of 1 MHz (Figure S12a, Supporting Information). The outer dimensions of the transducer are 50.8 mm in diameter and 38 mm in length, while the focal lens has a concave face, with a radius of curvature of 25 mm. These parts were assembled as designed (Figure S12b, Supporting Information), and the resulting transducer (Figure S12c, Supporting Information) was subjected to acoustic mapping by using a hydrophone scanning system. The acoustic field with the pressure distribution is shown in the *XY* (Figure S13a, Supporting Information) and *ZX* (Figure S13b, Supporting Information) planes, with the origin of the planes set at the point with the highest pressure value. The *XY* plane is parallel to the face of the transducer, while *Z* represents the axial direction of the transducer. Figure S13c (Supporting Information) shows the position of the origin, which is 25 mm from the surface of the transducer. The focal point with an elliptical shape is 2 mm in diameter and 10 mm in length (Figure S13a,b, Supporting Information). The HIFU produced with this transducer by applying a sine wave with a peak-to-peak voltage (V_{p-p}) of 0.6 V was highly powerful in that even durable PDMS rubber burned at the focal point (Movie S3 and Figure S13d, Supporting Information), while the material between the focal point and the surface of the transducer remained unchanged. Moreover, although a 3D-printed object fabricated by VP-3DP using a commercially available resin was a cross-linked polymer material in the glassy state, it was easily broken down in water (Movie S4 and Figure S14, Supporting Information). The observation through polarization films also allowed for the visualization of distortion inside the sample during HIFU sonication (Movie S4, Supporting Information). While applying a V_{p-p} of 0.6 V burned the test specimen at the focal region (Figure S15a, Supporting Information), lowering the energy of HIFU by varying V_{p-p} from 0.1 to 0.5 V allowed only distortion within the test specimens to be generated, as visualized by sandwiching the HIFU sonicated specimens with polarization films (Figure S15b, Supporting Information).

Having confirmed the effective conditions for examining the effect of HIFU on polymeric materials, we next performed HIFU sonication on **X**. From HIFU sonication tests with varying V_{p-p}, while specimens after HIFU sonication with a V_{p-p} of 0.2 V showed no visible changes, those with V_{p-p} of 0.4 and 0.6 V exhibited color changes derived from the production of TPIRs (**Figure 5a**) and distortion visualized with polarization films (Figure 5b). Time-course observation of HIFU sonication through the polarization films shows that the color change due to distortion first appeared inside the sample ($t < 5$ s), followed by color changes into blue ($t > 5$ s) (Movie S5, Supporting Information). The ESR spectrum of **X** validated that this blue color change is due to the formation of TPIRs by the appearance of the typical signal of TPIR (Figure 5c). If the cleavage of the covalent bonds occurs in polymer chains other than HABI-derived bonds, such an ESR spectrum would become complicated upon the formation of various types of radical species. To confirm this, we fabricated a control specimen (**C**) based on VP-3DP of a monomer mixture of only bis-GMA and MMA, and the fabricated **C** after HIFU sonication ($V_{p-p} = 0.6$ V) was subjected to ESR analysis. As clearly seen in the spectrum, fabricated **C** after HIFU sonication showed complicated signals in a broad magnetic field range (322–331 mT) (Figure S16, Supporting Information). Therefore, the ESR spectrum of **X** also demonstrates that the cleavage of the covalent bonds in

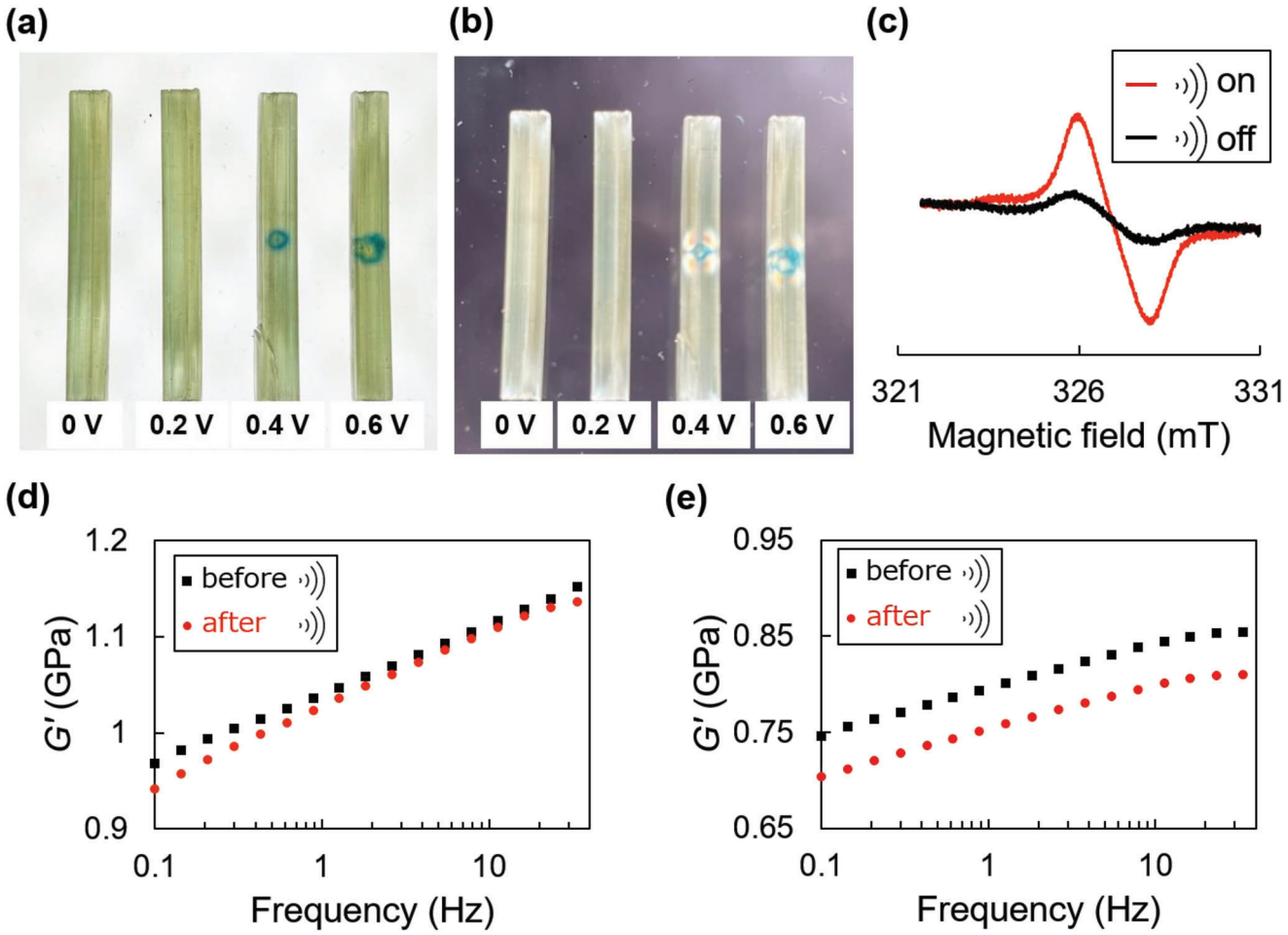

Figure 5. a) Photographs of 3D-printed test specimens of **X** before (0 V) and immediately after HIFU sonication for 15 s with a series of V_{p-p}s (0.2, 0.4, and 0.6 V) and b) their observation through polarization films. c) ESR spectra of **X** before (black line) and after (red line) HIFU sonication with the V_{p-p} of 0.4 V. d,e) Dependence of *G'* on frequency of **C** (d) and **X** (e) before (black squares) and immediately after HIFU sonication (red circles) with the V_{p-p} of 0.4 V.

polymer chains other than HABI-derived bonds can be negligible (Figure 5c). Moreover, these results indicate that the energy required to distort the interior of the glassy **X** is less than that required to cleave the covalent bonds between the two imidazoles of HABI within **X**.

From these investigations, it is clear that HIFU can not only burn materials but also reduce mechanical the properties of **X** without burning by decreasing its intensity. To quantitatively evaluate the effect of HIFU sonication on mechanical properties, we proceeded to measure the frequency dependence of *G'* before and after HIFU sonication. The *G'* of **C**, as a control specimen, before and after HIFU sonication was compared and found to decrease from 1.05 to 1.04 GPa at 1 Hz (Figure 5d). In contrast, the *G'* of **X** decreased from 0.80 to 0.75 GPa at 1 Hz (Figure 5e). This tendency was clearer at higher frequencies, e.g., at 10 Hz, there was little difference in *G'* before and after HIFU sonication to **C** (Figure 5d), but *G'* of **X** similarly decreased irrespective of frequency (Figure 5e). Importantly, the comparison of photographs taken immediately after HIFU sonication and light irradiation shows that the photoirradiated cuboid **X** shows coloration only on the surface (**Figure 6**a, right), whereas the HIFU-sonicated **X** shows internal coloration (Figure 6a, left).These observations are also shown schematically in Figure 6b. Hence, unprecedented remote control of the physical properties of the interior of materials and their visualization have simultaneously been realized by HIFU sonication of our DCMs. Taking into account the reversible nature of HABI (Figure 1a), it is important to show the reversibility of mechanical properties with **X** upon HIFU sonication. Thus, the HIFU-irradiated specimen in Figure 5a (V_{p-p} = 0.4 V) stored for 4 months were further subjected to DMA measurements. Although the TPIR-derived coloration has largely disappeared, the DMA measurement of the sample shows that *G'* remains decreased (Figure 6c, black circle). However, the TPIR-derived coloration appeared upon HIFU sonication of the specimen again (V_{p-p} = 0.4 V), and *G'* further decreased (Figure 6c, blue square). This indicates that, microscopically, the TPIRs reacted with each other and returned to HABI, but, macroscopically, the whole cross-linked network structure or the internal distortion caused by HIFU sonication was not relaxed at room temperature. Thus, to enhance the mobility of the entire polymer chain within the material, we conducted thermal treatment of the specimen at 50 °C for 30 min. The DMA analysis of the

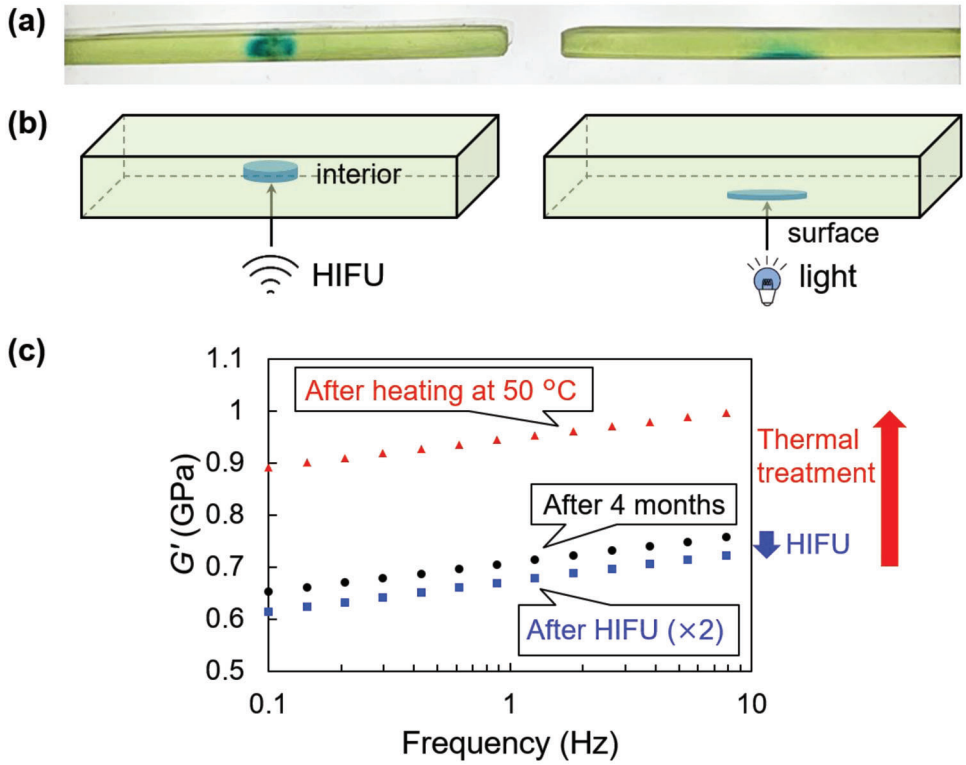

Figure 6. a) Side view photograph of the comparison of HIFU sonicated (V_{p-p} = 0.4 V) (left) and photoirradiated (right) 3D-printed test specimens of **X** and b) schematic illustrations of the responded areas upon HIFU sonication (left) and photoirradiation (right). Dependence of *G'* on frequency of **X** after the first HIFU sonication (V_{p-p} = 0.4 V) and stored for 4 months (black squares), immediately after the second HIFU sonication (V_{p-p} = 0.4 V) (blue rectangles), and after the heat treatment at 50 °C for 30 min (red circles).

thermally treated specimen showed that *G'* was even greater than that of the original specimen (Figure 6c, red triangle). In other words, it would be, in principle, possible to repetitively modulate mechanical properties by combining HIFU and heat as external stimuli.

Finally, by taking advantage of the fact that sound waves can travel even in the presence of obstacles, we have disclosed that **X** beyond the silicone obstacle responds to HIFU (Movie S6, Supporting Information), which cannot be attainable by photostimulation (Movie S7, Supporting Information).

3. Conclusion

Photo- and HIFU-responsive DCMs functionalized with HABIs in the chains have successfully been developed. Owing to the inert nature of TPIRs during photoinitiated free-radical polymerization conditions, the effective insertion of HABI-embedded cross-linkers into cross-linked polymeric materials upon VP-3DP has been achieved. While photostimulation only changes physical properties near the surface of the 3D-printed objects and allows the tuning of *G'*, HIFU is able to travel to the interior of the object as well and distort, break, or burn the material. Importantly, the excellent colorability of the generated TPIR enables the visualization of light-irradiated and HIFU-sonicated regions with the 3D-printed objects. The present acoustodynamic covalent materials engineering would be desirable for recyclable adhesives including human-body-related applications, where meticulous tuning of properties is needed. In addition, the marriage of DCMs and HIFU sonication systems will lead to the birth of sustainable new methodologies for pinpoint modification, healing, and reshaping of cross-linked polymeric materials that are generally insoluble and infusible. Since high output energy can be applied to the HIFU device to easily cause the burning of conventional polymers, this concept can be readily applicable to areas where disassembly of multiple parts joined together has been given up and discarded because of the use of conventional adhesives that cannot be dismantled. In addition, as revealed in this study, the established concept of acoustodynamic covalent materials engineering is highly compatible with VP-3DP. As the use of 3D printers expands explosively in the future to foster Industry 4.0 or Society 5.0, it can be used to manipulate physical properties and to reshape without discarding the 3D-printed objects only with the desired parts, thereby contributing to the realization of a sustainable future.

4. Experimental Section

Materials: All reagents and solvents were purchased from commercial sources (Fujifilm Wako and TCI) and used as received.

Photoinitiated Free-Radical Polymerization and VP-3DP: In a typical procedure, MMA (5.0 g, 50 mmol), **11** (0.25 g, 0.30 mmol), and TPO (348 mg, 1.0 mmol) were added to a vial, and the mixture was shaken

until complete dissolution. To this mixture, bis-GMA (4.75 g, 9.27 mmol) was added, and the mixture was stirred until a homogeneous oily solution was obtained. An aliquot was sandwiched on a pair of glass slides, and light (405 nm) was irradiated with a household LED lamp. The polymerization was qualitatively confirmed by the adhesion of the glass slides upon photocuring, and the remaining mixture was subjected to VP-3DP. Thus, a vat was filled with the remaining mixture and set on the LCD of the Lite3DP S1 3D printer equipped with an LED with an emission wavelength of 405 nm, and cuboid specimens (33 mm × 5 mm × 2 mm) were fabricated. The thickness of each layer was set at 50 µm, and the exposure times for the bottom and each layer were 75 and 45 s, respectively. The 3D-printed objects fabricated on the platform were thoroughly rinsed with isopropyl alcohol, dried in a nitrogen stream, and irradiated with light ($\lambda = 405$ nm) in an ANYCUBIC Cure and Wash Plus secondary curing machine for 5 min.

Photoirradiation Experiments: Photoirradiation during DMA analysis was performed on a Hamamatsu LIGHTNING CURE LC8 L9588 model with a Hamamatsu A10014-35-0110 light guide, and a Hamamatsu A9616-07 filter was used for transmitting UV light with a wavelength of 365 nm (150 mW cm^{-2}). For demonstration, a household LED lamp ($\lambda \approx 405$ nm) and blue laser pointer ($\lambda \approx 405$ nm) were also used.

HIFU Sonication Experiments: A HIFU transducer was fabricated from an aluminum lens, body, back cover, and PZT disk (ϕ25.0 mm, Fuji Ceramics Inc.) with a resonant frequency of 1 MHz as the components. The PZT disk was mounted on the opposite side of the lens, and the opposite side of the PZT disk was soldered to a sub-miniature A (SMA) plug. The SMA plug was connected to the output terminal of a ZCA5555 RF power amplifier (RAD corporation) with a rated power and gain of 200 W and +55 dB, respectively, where the input terminal was connected to a DF1906 function generator (NF corporation). HIFU sonication was performed by applying a sine wave (1 MHz) generated by the function generator to the device with a V_{p-p} of 0 to 0.6 V

Dynamic Mechanical Analysis: DMA measurements of 3D-printed objects with a rectangular shape (33 mm × 5 mm × 2 mm) were performed on an Anton Paar MCR 102 system in torsion mode. Strain (γ) sweep tests were first performed to find the linear viscoelastic region, and the measurements of specimens were conducted with a γ of 0.1%.

Supporting Information

Supporting Information is available from the Wiley Online Library or from the author.

Acknowledgements

The authors thank Ms. Yue Ji for her support in synthesizing cross-linkers. The author also thanks Prof. Taro Toyota (The University of Tokyo) for his kind support. This work was supported by JSPS KAKENHI (Grant Number 21H01632, S.H.), Fuji Seal Foundation (S.H.), the TEPCO Memorial Foundation, Research Grant (Basic Science) (S.H.), UTEC-UTokyo FSI Research Grant Program (S.H.), and Sao Paulo Research Foundation (FAPESP grant Number 2018/00710-1, C.N.P.). The authors are also grateful to the industrial collaborators for their financial support.

Conflict of Interest

The authors declare no competing financial interests.

Data Availability Statement

The data that support the findings of this study are available from the corresponding author upon reasonable request.

Keywords

cross-linked materials, dynamic covalent materials, high-intensity focused ultrasound, modulation of mechanical properties, vat-polymerization 3D printing

Received: May 2, 2023
Revised: June 19, 2023
Published online: July 20, 2023

[1] a) A. Bagheri, J. Jin, *ACS Appl. Polym. Mater.* **2019**, *1*, 593; b) Y. Bao, *Macromol. Rapid Commun.* **2022**, *43*, 2200202.
[2] a) A. Al Rashid, W. Ahmed, M. Y. Khalid, M. Koç, *Addit. Manuf.* **2021**, *47*, 102279; b) J. J. Tully, G. N. Meloni, *Anal. Chem.* **2020**, *92*, 14853.
[3] a) A. Salas, M. Zanatta, V. Sans, I. Roppolo, *ChemTexts* **2023**, *9*, 4; b) R. Daher, S. Ardu, E. di Bella, I. Krejci, O. Duc, *J. Prosthet. Dent.* **2022**.
[4] A. J. Boydston, B. Cao, A. Nelson, R. J. Ono, A. Saha, J. J. Schwartz, C. J. Thrasher, *J. Mater. Chem. A* **2018**, *6*, 20621.
[5] a) V. S. D. Voet, *ACS Mater. Au* **2023**, *3*, 18; b) A. Durand-Silva, K. P. Cortés-Guzmán, R. M. Johnson, S. D. Perera, S. D. Diwakara, R. A. Smaldone, *ACS Macro Lett.* **2021**, *10*, 486.
[6] M. Gernhardt, H. Frisch, A. Welle, R. Jones, M. Wegener, E. Blasco, C. Barner-Kowollik, *J. Mater. Chem. C* **2020**, *8*, 10993.
[7] a) S. Honda, T. Toyota, *Nat. Commun.* **2017**, *8*, 502; b) S. Honda, M. Oka, H. Takagi, T. Toyota, *Angew. Chem., Int. Ed.* **2019**, *58*, 144.
[8] R. Dessauer, in *Photochemistry, History and Commercial Applications of Hexaarylbiimidazoles*, (Ed: R. Dessauer), Elsevier Science B.V., Amsterdam, The Netherlands **2006**.
[9] a) T. Hayashi, K. Maeda, *Bull. Chem. Soc. Jpn.* **1960**, *33*, 565; b) G. R. Coraor, L. A. Cescon, R. Dessauer, A. S. Deutsch, H. L. Jackson, A. MacLachlan, K. Marcali, E. M. Potrafke, R. E. Read, *J. Org. Chem.* **1971**, *36*, 2267; c) G. R. Coraor, L. A. Cescon, R. Dessauer, E. F. Silversmith, E. J. Urban, *J. Org. Chem.* **1971**, *36*, 2262.
[10] a) Y.-C. Chen, Y.-T. Kuo, T.-H. Ho, *Photochem. Photobiol. Sci.* **2019**, *18*, 190; b) S. Berdzinski, N. Strehmel, H. Lindauer, V. Strehmel, B. Strehmel, *Photochem. Photobiol. Sci.* **2014**, *13*, 789.
[11] D. Ahn, S. S. Sathe, B. H. Clarkson, T. F. Scott, *Dent. Mater.* **2015**, *31*, 1075.
[12] Y. Ji, M. Oka, S. Honda, *Chem.: Methods* **2021**, *1*, 12.
[13] a) K. Mutoh, N. Miyashita, K. Arai, J. Abe, *J. Am. Chem. Soc.* **2019**, *141*, 5650; b) Y. Kishimoto, J. Abe, *J. Am. Chem. Soc.* **2009**, *131*, 4227.
[14] a) M. Oka, H. Takagi, T. Miyazawa, R. M. Waymouth, S. Honda, *Adv. Sci.* **2021**, *8*, 2101143; b) M. Oka, S. Honda, *Mater. Today Chem.* **2022**, *23*, 100727.
[15] R. Yao, J. Hu, W. Zhao, Y. Cheng, C. Feng, *J. Interv. Med.* **2022**, *5*, 127.
[16] M. Dellabella, A. Branchi, M. Di Rosa, M. Pucci, L. Gasparri, R. Claudini, F. Carnevali, S. Cecchini, D. Castellani, *Prostate Cancer Prostatic Dis.* **2021**, *24*, 1189.
[17] a) J. Xuan, O. Boissière, Y. Zhao, B. Yan, L. Tremblay, S. Lacelle, H. Xia, Y. Zhao, *Langmuir* **2012**, *28*, 16463; b) J. Wang, M. Pelletier, H. Zhang, H. Xia, Y. Zhao, *Langmuir* **2009**, *25*, 13201.
[18] J. Li, C. Nagamani, J. S. Moore, *Acc. Chem. Res.* **2015**, *48*, 2181.
[19] a) H.-A. Klok, A. Herrmann, R. Göstl, *ACS Polym. Au* **2022**, *2*, 208; b) B. A. Versaw, T. Zeng, X. Hu, M. J. Robb, *J. Am. Chem. Soc.* **2021**, *143*, 21461.
[20] V. M. Lau, A. J. Halmes, M. L. Oelze, J. S. Moore, K. C. Li, *Proc. Natl. Acad. Sci. USA* **2019**, *116*, 10214.
[21] G. Kim, Q. Wu, J. L. Chu, E. J. Smith, M. L. Oelze, J. S. Moore, K. C. Li, *Proc. Natl. Acad. Sci. USA* **2022**, *119*, e2109791119.
[22] D.-H. Shin, H. R. Rawls, *Dent. Mater.* **2009**, *25*, 1030.